

INTERNATIONAL JOURNAL CONSERVATION SCIENCE

ROMANIA WWW.ijcs.ro

ISSN: 2067-533X Volume 16, Issue 4, 2025: 1723-1738

DOI: 10. 36868/IJCS.2025.04.07

BEYOND THE GOLDEN GLOW: ANALYTICAL STUDY OF MURAL PAINTINGS AND STUCCOES IN THE PALATINE CHAPEL OF S. ANNA

Francesco ARMETTA^{1,2}, Salvatore BARRECA^{3*}, Giovanni ARENA³, Diana AMORELLO¹, Laura BARRECA^{4,5}, Santino ORECCHIO¹, Silvia ORECCHIO⁶

¹Department of Biological, Chemical and Pharmaceutical Sciences and Technologies (STEBICEF), University of Palermo, Viale delle Scienze, Palermo, Italy

² IPCF-CNR, Istituto per i Processi Chimico Fisici, V.le F. S. d'Alcontres 37, I- 98158 Messina, Italy 1
³ Department of Chemical Sciences, University of Catania, Viale A. Doria 6, Catania, 95125, Italy
⁴ Museo civico Castelbuono, Piazza Castello, 3, 90013 Castelbuono PA, Italy

⁵ Accademia di Belle Arti Catania via del Bosco, 34/a 95125 Catania, Italy

⁶ Department of Physics and Chemistry Emilio Segrè, Viale delle Scienze, 90100 Palermo, Italy

Abstract

This study examines the chemical composition of wall paintings and stucco work in the Palatine Chapel of S. Anna, housed within the Ventimiglia Castle of Castelbuono, Sicily. Employing non-destructive techniques such as X-ray fluorescence (XRF), Fourier transform infrared (FT-IR) spectroscopy, and X-ray diffraction (XRD), the research identifies the pigments and materials used in the chapel's decorations. The analyses have found that the iconic golden yellow background primarily consists of lead- and iron-based pigments, with traces of gold. The stucco analysis revealed a composition characteristic of the Serpotta school, predominantly featuring calcite, gypsum, and minor quartz. Additionally, indoor dust analysis detected significant lead levels, raising concerns about environmental impact and cultural heritage preservation. These findings provide essential insights for conservation strategies and deepen the understanding of the chapel's artistic and historical significance.

Keywords: Mural painting; Characterization in cultural heritage; Serpotta creation; Indoor dust analyses

Introduction

Chemical analyses of wall paintings are vital in the conservation, restoration, and appreciation of cultural heritage [1-5]. These artistic artifacts, such as frescoes and other forms of pictorial wall art, hold immense historical and cultural value. By studying their chemical and physical properties, researchers can uncover the materials, techniques, and technologies used across various historical periods [6]. Such analyses not only aid in preservation but also serve to enhance public engagement through exhibitions, publications, and educational programs. Although Italy can be considered as one of the most important nations in the context of cultural heritage sites, has seen limited application of scientific research techniques in heritage conservation has seen limited application of scientific research techniques in heritage conservation [4].

^{*} Corresponding author: salvatore.barreca@unict.it

In this context, the research project "Observing to preserve the Palatine Chapel of S. Anna in the Ventimiglia Castle of Castelbuono" (OSANNA) aims at the scientific study of the paintings and stuccos of this chapel located inside the Castle of Castelbuono. Castelbuono is a little city of 10000 people, situated about 420 meters above sea level, in the beautiful and lush Madonie Park and located in the northern part of the island of Sicily, an Italian region, which is the largest island in the Mediterranean Sea. The town's roots can be attributed to the Ventimiglia family, nobles hailing from the nearby County of Geraci, who built the castle that lends its name to the settlement. The Ventimiglia Castle, also known as Castelbuono Castle, is the symbol of the medieval village built on the site of an ancient Byzantine farmhouse known as Ypsigro. Castelbuono's architectural heritage offers invaluable insights into prevailing artistic trends, religious practices, and socio-political dynamics of bygone eras. One of the most important monuments of Castelbuono is the Palatine Chapel of Sant'Anna, located inside the castle and decorated with elaborate stuccoes by the Serpottian school, manufactured against a yellow background. This type of yellow background for Serpota sculptures represents a uniqueness. Some studies have been carried out on the Serpotta stuccos [8-9]; however, as far as we know, no chemical analyses have been reported for the Palatine Chapel of Castelbuono.

Generally, for the stucco technique, artists opted for mortars over marble due to their significantly lower cost and the ease with which lime plasters could be moulded into various shapes [8]. Stucco art is regarded as one of the key expressions of Baroque decorative art in Sicily, with the Serpotta family being particularly prominent, and their statues give the impression of floating, even though all elements are flush with the wall. Imaging of the Palatine Chapel of Saint Anna is reported in Figure 1.

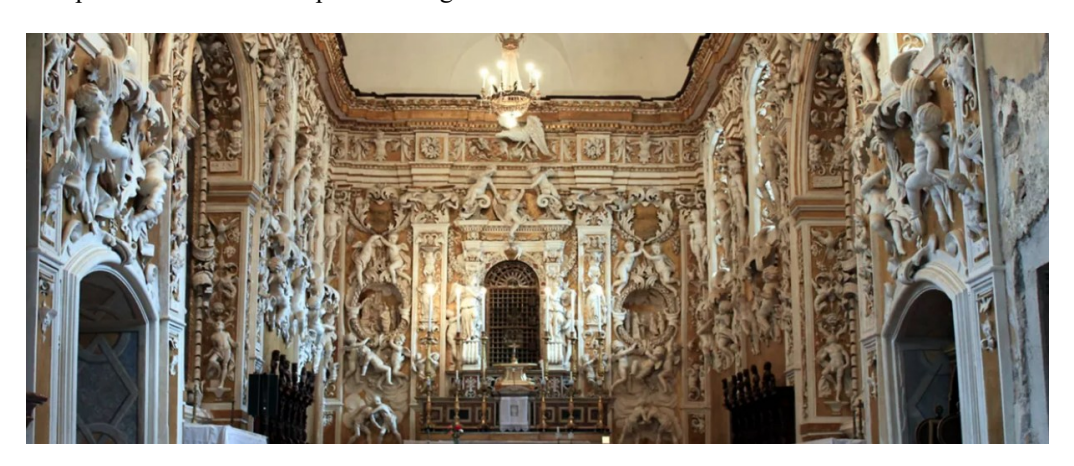


Fig. 1. The S. Anna palatine chapel inside the castle of Castelbuono

The Church of Saint Anna stands as a timeless testament to the region's rich history. Dating back to the medieval era, this architectural gem is not only a place of worship but also a symbol of artistic and cultural heritage. For these reasons, the chemical characterization of its manufactured goods has a significant impact, not only in the field of cultural heritage but also in the context of citizen science.

Indeed, most of the visitors, thrilled to see the statues against the golden yellow background, wonder if the walls of the church are effectively covered in gold. In this context, the chemical characterization of mural painting and Serpotta's stuccos will provide important information for researchers and citizen scientists.

Identifying the elements in the colorants used in ancient works of art is important from the [8-9] historical perspective, as well as for the restoration and reproduction of the artwork; identifying the elements in colorants is crucial. Pigments are among the most intriguing

materials to study, as ancient painters, to obtain the desired color or shade, made use of several natural or artificial substances. The pigment identification could be resolved by the use of several chemical techniques [10-12]; some of them require big amounts of samples. The prerequisite of superintendence of cultural heritage and curators for the use of non- or low-destructive analytical techniques during the examination of ancient material makes X-ray fluorescence spectrometry (XRF) technique an important tool for the analysis of the cultural heritage. In this research, XRF was used directly in situ to identify the elements present in the paint layers [13-15], while, to obtain information on the preservation of cultural heritage from chemical substances, voltammetry and gas chromatographic analyses were performed in indoor dust used as a passive sampler for the determination of some heavy metals and polycyclic aromatic hydrocarbons, respectively. Indeed, indoor environments can be polluted by platinum dust in several ways: as access from outdoor environments, in particular, from vehicle emissions; from atmospheric outdoor particulate by wind or shoes; and, at the present time, it is well known that car converters are the major source of emission of platinum into the environment [16-17].

On the other hand, candle, wood, and/or fossil combustion are sources of polycyclic aromatic hydrocarbons (PAHs), and these environmental pollutants represent a class of aromatic compounds forming during incomplete combustion [18-20]. Once absorbed by materials, they tend to accumulate [21-22] and are likely to persist for a long time due to their stability, low water solubility, and hydrophobicity, especially in organic matrices like wood. PAHs can also be found in various matrices, such as the atmosphere [23-24], water [25-28], soil and sediments [29-34], but unfortunately, information about the distribution of these pollutants in ancient materials is rare [35-38], also by considering the analytical difficulties that may occur with archaeological or historical materials.

Summing up, the primary goal of this study is to conduct an analytical investigation of the materials constituting the stuccoes and pigments to determine whether the yellow colors are attributed to gold or other types of inorganic pigments.

Experimental part

Materials

All reagents used were of analytical grade. Hexane, heptane, acetone, and dichloromethane were employed for sample preparation.

A PAHs standard solution containing 20 compounds ($500\mu g/mL$) was sourced from Supelco (Milano). Calibration standards ranged from 0.3 to $50\mu g/L$, prepared with internal standards and stored at 4°C to avoid degradation. Standard stock solutions of Pt and Pb ($1000\mu g/mL$) were supplied by Fluka (Milano).

Solutions were freshly prepared to maintain accuracy.

X-ray Fluorescence (XRF) spectra were obtained using a Tracer III SD Bruker AXS portable spectrometer with a Rhodium target X-ray tube, operating at 40 kV and 11 μ A. The data was analyzed using 1PXRF® and ARTAX 7 software. Fourier-Transform Infrared (FT-IR) Spectroscopy was obtained by using the μ FT-IR Lumos Bruker spectrophotometer with a germanium ATR crystal, which was used to analyze samples within a spectral range of 4000–700 cm⁻¹.

X-ray Diffraction (XRD) analyses were performed by a Philips PW 1050/39 diffractometer employed to determine mineralogical compositions. The Rietveld refinement method was applied for quantitative analysis using HighScore® software.

Voltammetry and Gas Chromatography analyses were performed by Differential Pulse Voltammetry (DPV/a) and GC-MS techniques used to quantify platinum, lead, and PAHs in dust samples.

A PAHs standard solution containing 20 compounds at $500\mu g/mL$ (PHAs Mix) was supplied by Supelco (Milano). Calibration standard solutions, with concentrations ranging from 0.3 to $50\mu g/L$, were prepared by diluting the stock solution with a mixture containing two internal standards. Both the stock and calibration standard solutions were stored in a refrigerator at 4°C to avoid PAH degradation [19].

Standard stock solutions of Pt and Pb ($1000\mu g/mL$) were obtained from Fluka (Milano, Italy), and diluted solutions were prepared daily. All reagents, including HNO₃ (65%) and HCl (37%) from Suprapur Carlo Erba (Milano, Italy), were of analytical grade. Daily preparations of hydrazine and formaldehyde solutions were made using analytical-grade reagents from Carlo Erba (Milano, Italy). Milli-Q water was used for all solution preparations.

XRF spectra were obtained utilizing a Tracer III SD Bruker AXS portable spectrometer. This involved irradiation by a Rhodium Target X-ray tube operating at 40kV and 11 μ A, with fluorescence X-rays detected by a 10mm² silicon drift X-Flash detector, allowing the detection of elements with atomic number Z > 11. A sampling area of 3-4mm in diameter was defined by a window. Each spectrum was acquired over a period of 30 seconds. Data acquisition and spectral assignment were performed using the S1PXRF® software (accessed via https://s1pxrf.software.informer.com/ on 14 April 2023). The fluorescence signal area was estimated after deconvolution of the entire spectrum using ARTAX 7 software. Additionally, signals from atmospheric Ni, Ar, Rh, and Pd, originating from instrumental components, were present in all spectra.

The micro-FT-IR spectra were recorded using a µFT-IR Lumos Bruker spectrophotometer with a germanium ATR crystal. Spectral data were acquired over a range of 4000 to 700cm⁻¹, with a spectral resolution of 2cm⁻¹ and a scan rate of 120 scans. The area analyzed was approximately 50 microns in size, based on the dimensions of the crystal tip. A baseline correction for scattering was applied to all spectra, and the data were analyzed using OPUS 7.5® software. The stone support and mortars were analyzed using X-Ray Diffractometry (XRD) to determine their mineralogical composition. XRD patterns were obtained with a Philips PW 1050/39 diffractometer configured in the Bragg-Brentano geometry, utilizing Ni-filtered Cu K α radiation ($\lambda = 1.54056$ Å). The data were collected over a 2 θ range of 5-90° with a step size of 0.05° and an acquisition time of 5 seconds per step. The X-ray generator operated at 40kV and 30mA, and the instrument's resolution (with divergent and antiscatter slits of 0.5°) was calibrated using R-SiO2 and R-Al2O3 standards, ensuring no influence from reduced crystallite size or lattice defects. Phase identification was conducted using X'pert HighScore® Software and compared against spectra from the RRUFFTM Project database; the quantification was performed with the same software by using the RIETVELD refinement.

The pigments were investigated by X-ray Fluorescence (XRF), (pigments and inerts) and by Fourier-transform Infrared Spectroscopy (FT-IR) The spectral assignments of the characteristic peaks of an element were carried out using the database contained in the ARTAX 8 software. In each spectrum, the signals of Rhodium (Rh) and Argon (Ar), due to the source and the atmosphere, respectively, are present.

For the Attenuated Total Reflectance (ATR) FT-IR measurements, a Bruker Vertex 70 Advanced Research FT-IR Spectrometer was utilized for analysis. Equipped with a Platinum ATR and a diamond crystal, it measured samples over a range of 4000-700cm⁻¹ with a step size of 2cm⁻¹. Measurements were conducted using 200 scans at 2hPa on a small quantity of powdered sample. FORS spectra were acquired in situ through a UV–VIS–NIR Ocean Optics portable fiber-optic spectrometer. The instrument used is equipped with a DH mini light source, a detector operating in the spectral range 350–1100nm (USB 2000 + XR1), and a reflection

bifurcated probe, in which seven illumination fibers are installed around a central reading fiber, providing illumination and detection of diffused light from the same direction.

Quantification of Pt and Pb in dust samples was carried out by Differential Pulse Voltammetry (DPV/a) using the standard addition procedure, following a procedure set up and optimized in previous research [16-17]. All voltammetric analyses were carried out using an AMEL Polarograph with 8.60 software for storing and processing data.

The solutions containing platinum chloride complexes (H₂PtCl₄, PtCl₄²⁻) were purged with high-grade nitrogen (99.998%) for 300 seconds at the beginning of each measurement, and a continuous flow of gas was maintained over the solution throughout the measurement to prevent interference from oxygen. All experiments were conducted at a constant temperature of 25°C. Platinum analysis was performed in a 1.0M sulfuric acid supporting electrolyte, with the addition of 1.2mM hydrazine sulfate and 0.6mM formaldehyde. In situ, formaldehyde and hydrazine react to form the corresponding hydrazone, which subsequently complexes with Pt. A potential ranging from -0.3 to -1.0V was applied to the working electrode in differential pulse mode, and the catalytic current for hydrogen development was measured at -0.85V (versus Ag/AgCl). The intensity of this current is proportional to the platinum concentration [16-17], highlighting the extreme sensitivity of this determination due to the catalytic effect of Pt. Analyses of PAH were performed by using a Gas-Chromatography coupled with mass spectrometry (GC-MS) GC 9000 intuvo MSD 5977B Agilent.

Sampling and analyses for chemical characterization

The sampling campaign was carried out under the supervision of the assistants of Museo Civico Castelbuono. Analysis was performed both on-site and off-site on fragments from detachments found during operation measures. Non-destructive XRF analyses were performed directly on the surface of paint and plaster of the mural paints for a total of 8 spot samples. In Table 1 are shown details of original locations and brief descriptions. In cases where several samples were present, each was given an alphanumeric ID associated with a sequential letter.

Spot sample ID	Sampling point	Description
01 White	Church of S. Anna, Castelbuono. Allegoric statue, from (culmination, lower part, right side)	White layer of statue
02 Yellow	Church of S. Anna, Castelbuono. Mural painting sampled in North part of the church	Yellow/brown layer of mural
03 Yellow	Church of S. Anna, Castelbuono. Mural painting sampled in East part of the church	yellow layer of mural
04 Yellow restored	Church of S. Anna, Castelbuono. Mural painting sampled in East part of the church	Restored area
05 Yellow restored	Church of S. Anna, Castelbuono. Mural painting sampled in East part of the church	Restored area
06 Golden bottom	Church of S. Anna, Castelbuono. Mural painting sampled in the main chapel	Light Golden area inner the human touching zone
07 Golden bottom	Church of S. Anna, Castelbuono. Mural painting sampled in the main chapel	Light Golden area inner the human touching zone
08 Golden up	Church of S. Anna, Castelbuono. Mural painting sampled in the main chapel	Golden area out of the human touching zone

Table 1. Description of the collected spot samples

The sampling areas considered include Panel A (located in the northwest area of the chapel) and Panel B (located in the northeast area of the chapel). A schematic representation of sampling sites is reported in Figure 2.

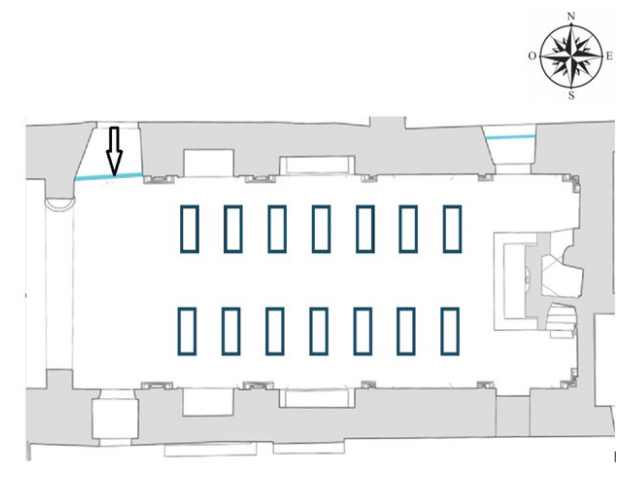


Fig. 2. Schematic representation of S. Anna palatine chapel with sampled point

Table 2. Chemical characterization by Py-GC/MS, FTIR, Raman and SEM-EDS, indicating paint origin, color, medium, and elemental analysis

Sample	Origin	Color	Medium	Elements
Acrilex	BRA	BPc	PS	Al, Si, S, Cu, Ti
Corfix	BRA	BPc	PS	Si, S, Cu, Ti
Corfix Arts	BRA	BPc	P(S/MA)	Al, Si, S, Ca, Cu, Ti, Ce
Liquitex	USA	BPc	P(nBA/MMA)	Al, S, Ca, Cu
Acrilex	BRA	BPr	PS	Na, Mg, Al, Si, S, Ca, Fe
Corfix	BRA	BPr	PS	Na, Al, Si, S, Cu
Corfix Arts	BRA	BPr	P(S/MA)	Na, Al, Si, S, Fe, Ti, Ce
Winsor & Newton	GBR	BPr	P(S/MMA)	Na, Al, Si, S, K, Ca, Fe

Methods

About dust analyses, 6g of settled dust samples from two sampling targets (S1 and S2). The samples were carefully collected using brushes from surfaces positioned 1.5–2.0m above ground level, typically at the surface of the furniture, to minimize the inclusion of foreign coarse materials. They were refrigerated at 4°C on-site until they could be rapidly transported to the laboratory, where they were subsequently frozen before analysis. Among different techniques and solvents tested in previous works, we used the ultrasound bath extraction because it allowed us to obtain the highest recovery percentage of PAHs. About 2.5 g of dried and pulverized sample was mixed with precleaned anhydrous Na₂SO₄ (Carlo Erba, Milano). The samples were extracted three times in an ultrasonic bath for 30 minutes each time, using a 20mL mixture of dichloromethane and pentane in a 1:1 ratio. The extracted samples were then filtered through a pre-cleaned pipette filled with solvent-rinsed glass wool and anhydrous Na₂SO₄. After filtering, the samples were rinsed and concentrated using a rotary evaporator set to a thermostatic bath temperature of 35 (±0.5)°C, resulting in a final volume of 2.5mL. The solution containing PAHs was subsequently dried under a gentle nitrogen flow. The dry residue was reconstituted in 200µL of an internal standard solution containing phenanthrene d10, acenaphthene d10, perylene d12, and chrysene d12 at a concentration of 500mg/L. One microliter of each extract was injected in splitless mode into a gas chromatograph fitted with a 30 m Equity-5 fused silica capillary column (0.25mm×0.25m film thickness) and connected to a mass spectrometry detector. The carrier gas was helium, maintained at a flow rate of 1.4mL/min. The injection port temperature was 280°C. The detector was 325°C. The oven program for standards and samples was as follows: 60°C for 2min, 14.5°C/min up to 325°C for 13min, respectively.

For Pt and Pb quantification, about 250mg of dust, in a porcelain crucible, was ashed in a muffle at 550°C. After cooling, the ashes were treated with 1mL of hot HNO₃ + HCl (1:3) in a Milestone model MLS-1200 Mega (Milestone Laboratory Systems, Italy) microwave oven, equipped with high-pressure (up to 100 bar) Teflon containers. The instrumental conditions used for the microwave digestion were 1min at 250W, 1min at 0W, 5min at 250W, 5min at 450W, 3min at 600W and 5min at 300W. After digestion, the clear, colorless solution was brought to volume with Milli-Q water.

Results and discussion

Mural Painting Characterization and Stucco Analysis

The chemical analysis revealed variations in the composition of yellow pigments across restoration and original areas. XRF spectra indicated that older yellow regions contained lead, calcium, and iron, while restored areas showed calcium, iron, and zinc, with reduced lead levels. The gold regions displayed small amounts of gold with prominent lead signals, highlighting human contact's impact on gold content. FT-IR spectroscopy identified calcite, gypsum, and organic compounds within the yellow pigments. XRD confirmed the presence of iron oxide and litharge as the main components, consistent with historical pigment formulations.

The stucco composition, determined by XRD, predominantly consisted of calcite (57.6%) and gypsum (34.3%), with minor contributions from quartz (2%). These findings align with other studies on Serpotta's works, reinforcing its attribution to this renowned Baroque artist. The dust analysis revealed significant PAH levels, with fluoranthene, pyrene, and chrysene being the most abundant components. PAH ratios suggested high-temperature combustion as the primary source. Lead concentrations in dust samples were markedly higher than platinum, indicating plaster particulate release and raising concerns for preservation efforts.

During the inspection conducted inside the church, even if there is a general golden view, different shades of yellow were observed in the background, which we categorized as restoration yellow, old yellow, and gold. To determine the chemical composition of the background, XRF spectra were obtained from four different background colors: yellow restoration, yellow, and gold. Furthermore, the contribution of the preparation layer was taken into account by analyzing a white area uncovered by the yellow pigments. Analyses were conducted on various sample plots, and the representative spectra are presented in Figure 3.

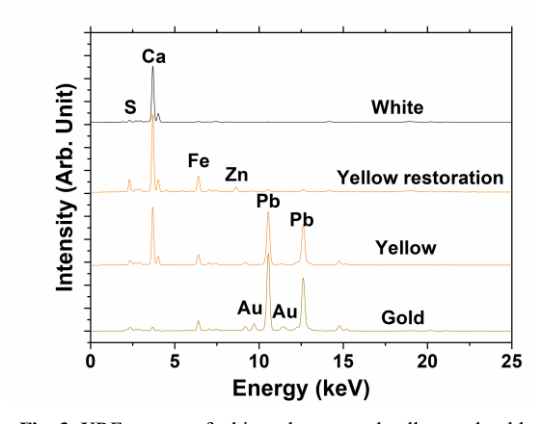


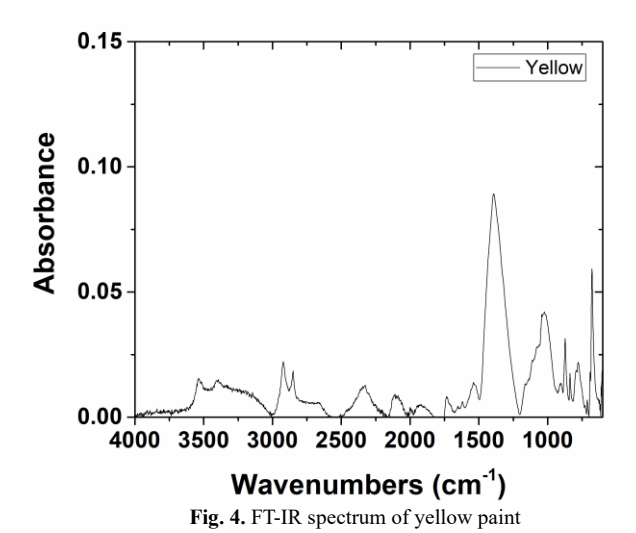
Fig. 3. XRF spectra of white substrate and yellow and golden areas

The white preparation layer is characterized by the presence of calcium (Ca), attributed to calcium carbonate (calcite) and/or gypsum. Elemental analysis of the yellow

background revealed three distinct compositions. The older yellow area contains lead (Pb), calcium (Ca), and iron (Fe), whereas the yellow restoration pigment is composed of calcium (Ca), iron (Fe), and zinc (Zn), with only trace amounts of lead (Pb). This variation in elemental composition suggests the use of different pigments during a restoration process. Specifically, the replacement of lead, likely due to its toxicity, with other inorganic or organic materials supports the conclusion that the yellow pigment was subjected to restoration. In both areas, the calcium signals may be associated with the intentional addition of calcite or gypsum to the pigment mixture.

Spectral analysis of the gold-colored area detected small quantities of gold, with lead signals remaining dominant. Measurements taken from the accessible portions of the wall revealed a lower gold content compared to measurements from higher regions. Quantification using the peak area ratio between gold and lead yielded values of 0.11 for the upper areas and 0.05 for the lower areas, indicating a relatively higher gold content at elevated locations. This gradient is likely attributable to the gradual removal of gold in the lower regions due to frequent human contact.

Figure 4 shows the FT-IR spectrum of the sample from the yellow area, where the most significant peaks of calcite (713cm⁻¹, 875cm⁻¹ and 1425cm⁻¹) can be recognized together with some signals typical of the vibration mode of sulfate in gypsum (3600 to 3200cm⁻¹, 1683cm⁻¹, 1620cm⁻¹ and 1108cm⁻¹), and of an organic material characterized by the stretching of aliphatic groups (C-H 2900cm⁻¹) and a carbonyl group (C=O 1735cm⁻¹). The spectral region around 2200-2000cm⁻¹ exhibits characteristic auto-absorption features of the diamond crystal, making it impossible to identify the sample's characteristic signals. Unfortunately, due to the limited amount of available samples, the signal-to-noise ratio of both the FT-IR spectrum and the diffraction curve is low, and the baseline correction does not significantly improve the readability of the curves.



In order to better discriminate the type and composition of crystal of compound containing lead, X-ray diffraction analysis (XRD) was performed, and, in addition to a broad amorphous band due to non-crystalline compounds, the presence of several characteristic peaks of crystalline phases of iron oxide (Ir) and litharge (Ly) can also be observed, confirming the

use of these pigments (see Figure 5).

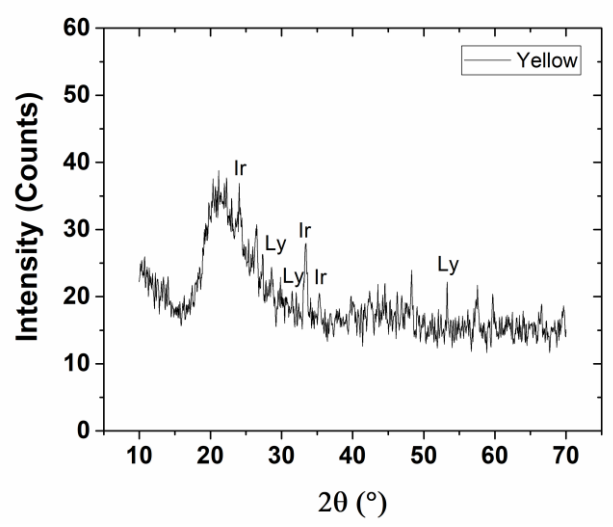


Fig. 5. XRD pattern obtained from a sample of yellow paint. The crystal phases correspond to Iron oxide (Ir) (Ref Code 01-084-0308) and Litharge (Ly) (Ref Code 03-065-0399)

Figure 6 summarizes the compositions obtained through XRD pattern obtained from sample of plaster (detaching). The fragment of detaching is characterized by gypsum (Gy), quartz (Q), anhydrite (An), and calcite (Ca). It is interesting to note that calcite (Ca) is the most abundant component (57.6%), followed by gypsum (Gy, 34.3%), anhydrite (An, 6.1%), and quartz (Q, 2%). These data are in good agreement with other studies of the composition of Serpotta's stucco, which report a similar distribution of components [6].

Figure 7 shows the FT-IR spectra of the plaster sample, comparing it with calcium carbonate and gypsum, and the overlayered peaks from 1409cm⁻¹, 1090cm⁻¹, 874cm⁻¹ and 725cm⁻¹ can be attributed to calcium carbonate (in the form of the calcite phase), and the peaks from 3600 to 3200cm⁻¹, 1683cm⁻¹, 1620cm⁻¹, 667cm⁻¹ and an intense peak at 1108cm⁻¹ confirm the presence of gypsum in the plaster samples as a result of a mixture of the two minerals. Moreover, the absence of other peaks excludes the presence of organic substances as ligands.

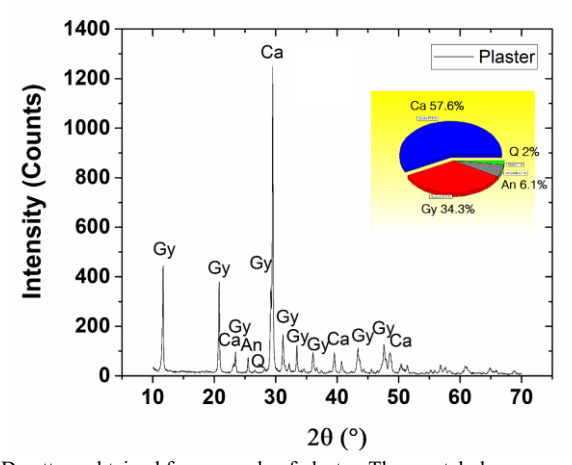


Fig. 6. XRD pattern obtained from sample of plaster. The crystal phases correspond to Gypsum (Gy) (Ref Code 01-072-0596), Quartz (Q) (Ref Code 01-087-2096), Anhydrite (An) (Ref Code 01-086-2270), and Calcite (Ca) (Ref Code 01-086-2335). Inset, weight percentage of the identified phases

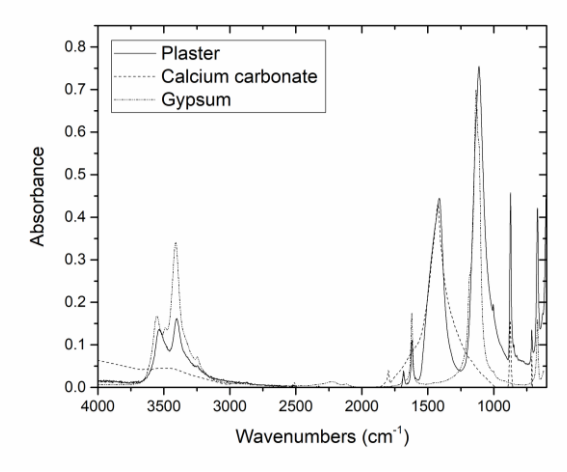


Fig. 7. FT-IR spectrum of plaster sample compared to Calcium carbonate and Gypsum references

These results provide scientific confirmation of the origin of the sculpture attributed to Serpotta's school.

Dust samples analyses

Table 3 summarizes the results obtained for analyzed dust samples collected while the percentage of PAHs distribution is reported in Figure 8.

Table 3. PAH, Pb and Pt analyses performed on indoor dust samples

Analyte	LOQ	Sample	Sample	Mean
11yic	Log	SI SI	S2	17101111
	μg L ⁻¹	$(\mu g L^{-1})$	$(\mu g L^{-l})$	$\mu g L^{-1}$
Naphthene	0.3	4.88	9.60	7.24
Acenaphthene	$0.3~\mu g~L^{-1}$	<loq< td=""><td><loq< td=""><td><loq< td=""></loq<></td></loq<></td></loq<>	<loq< td=""><td><loq< td=""></loq<></td></loq<>	<loq< td=""></loq<>
Acenaphthylene	0.3 μg L ⁻¹	<loq< td=""><td><loq< td=""><td><loq< td=""></loq<></td></loq<></td></loq<>	<loq< td=""><td><loq< td=""></loq<></td></loq<>	<loq< td=""></loq<>
Fluorene	$0.3~\mu g~L^{-1}$	0.76	0.76	0.76
Phenanthrene	0.3 μg L ⁻¹	11.89	11.13	11.51
Anthracene	$0.3~\mu g~L^{-1}$	1.07	0.61	0.84
Fluoranthene	0.3 μg L ⁻¹	15.85	21.04	18.45
Pyrene	0.3 μg L ⁻¹	12.96	12.50	12.73
Benzo[a]anthracene	0.3 μg L ⁻¹	3.51	4.27	3.89
Chrysene	0.3 μg L ⁻¹	13.42	14.03	13.72
Benzo[b.k.i]anthracene	0.3 μg L ⁻¹	<loq< td=""><td>7.47</td><td>3.74</td></loq<>	7.47	3.74
Benzo[e]pyrene	0.3 μg L ⁻¹	5.03	5.64	5.34
Benzo[a]pyrene	0.3 μg L ⁻¹	2.59	6.10	4.34
Perylene	0.3 μg L ⁻¹	<loq< td=""><td>1.07</td><td>0.53</td></loq<>	1.07	0.53
Benzo[g.h.i]perylene	0.3 μg L ⁻¹	0.46	2.13	1.30
Dibenzo[a.h]anthracene	$0.3~\mu g~L^{-1}$	<loq< td=""><td><loq< td=""><td><loq< td=""></loq<></td></loq<></td></loq<>	<loq< td=""><td><loq< td=""></loq<></td></loq<>	<loq< td=""></loq<>
Indeno[1.2.3-c.d]pyrene	$0.3~\mu g~L^{-1}$	2.74	2.52	2.63
benzo[j]fluoranthene	0.3 μg L ⁻¹	<loq< td=""><td><loq< td=""><td><loq< td=""></loq<></td></loq<></td></loq<>	<loq< td=""><td><loq< td=""></loq<></td></loq<>	<loq< td=""></loq<>
benzo[k]fluoranthene	0.3 μg L ⁻¹	<loq< td=""><td><loq< td=""><td><loq< td=""></loq<></td></loq<></td></loq<>	<loq< td=""><td><loq< td=""></loq<></td></loq<>	<loq< td=""></loq<>
benzo[b]fluoranthene	0.3 μg L ⁻¹	<loq< td=""><td><loq< td=""><td><loq< td=""></loq<></td></loq<></td></loq<>	<loq< td=""><td><loq< td=""></loq<></td></loq<>	<loq< td=""></loq<>
TOTAL PAH		75.16	98.86	87.01
	(µg g ⁻¹)	$(\mu g g^{-1})$	$(\mu g g^{-1})$	$(\mu g g^{-1})$
Pt (µg g ⁻¹)	0.01	0.29	0.38	0.34
Pb (mg g ⁻¹)	0.001	0.22	0.33	0.28

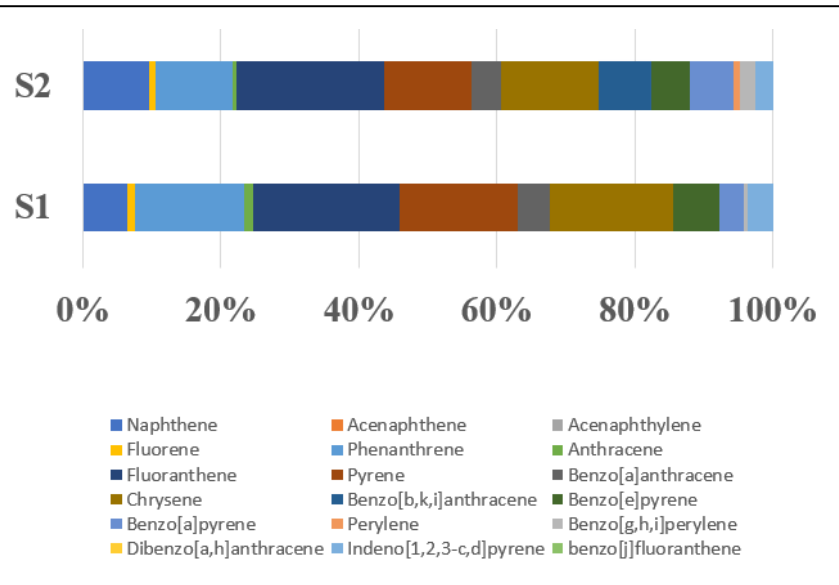


Fig. 8. PHAs percental distribution in indoor dust samples

For each of two analyzed samples, fluoranthene, pyrene, and chrysene are the three most abundant components. It is interesting to note that the PAH percentage distribution in the samples is very similar. Generally, the composition of PAH emissions varies depending on the source. To investigate sources of the PAHs in the samples, different PAHs ratios were calculated and discussed by literature comparison.

Generally, PAHs of molecular mass 178 and 202 are used to discriminate between combustion and petroleum sources [39]. In the two analyzed dust samples, the ratios of anthracene to anthracene plus phenanthrene An/(An+Ph) are 0.08 and 0.05 for S1 and S2, respectively. A ratio of 0.10 usually indicates that the PAHs can originate from low-temperature sources (petroleum), while a ratio > 0.10 indicates a dominance of combustion [40].

Another PAHs ratio used to investigate PAH sources is fluoranthene versus pyrene, and for the analyzed samples, Fl/(Fl+Py) ratios are 0.55 for sample S1 and 0.63 for sample S2. Typically, literature reported that the Fl/(Fl+Py) ratio is below 0.50 for most petroleum samples and for diesel, fuel oil combustion, gasoline, and emissions from cars [41] and above 0.50 in grass, most coal, and wood combustion. In detail, vehicle and crude oil combustions are more uniform, ranging from 0.41 to 0.49, and are closer to the 0.50 boundary than those from diesel exhaust. The petroleum limit ratio for Fl/(Fl+Py) tends to be closer to 0.40 rather than 0.50. Ratios between 0.40 and 0.50 are more indicative of liquid fossil fuel combustion (such as from vehicles and crude oil), while ratios greater than 0.50 are characteristic of combustion from grass, wood, or coal.

More precise identification of PAH sources can be achieved using additional, different isomer ratios. PAHs with a molecular mass of 228 are rarely employed as indicators of parent PAHs. According to data from the literature [41], BaA/(BaA+Chr) ratios below 0.20 suggest petroleum emission, ratios between 0.20 and 0.35 can indicate either petroleum or combustion, and ratios above 0.35 imply combustion products. According to literature data (Hischenhuber and Stijve, 1987), IP/(IP + BghiP) ratios of 0.20 most likely imply a petroleum origin, and between 0.20 and 0.50, liquid fossil fuel combustion (vehicle and crude oil).

According to literature data [38-41], IP/(IP+BghiP) ratios between 0.20 and 0.50 imply liquid fossil fuel combustion, and ratios >0.50 imply grass, wood, and coal combustion. In the analyzed samples, IP/(IP+BghiP) ratios for S1 and S2 are 0.86 and 0.54, respectively.

Finally, we calculated the total index as the sum of single indexes (discussed before) respectively normalized for the limit value (low-temperature sources and high-temperature sources) reported in literature.

In detail, the total index was calculated as reported in Eq. 1, and the results are reported in Table 4.

Total index = FI/(FI+ Py)/0.4 + An/(An + Ph)/0.2 + B[a]A/(B[a] A + Chr)/0.1 + IP/(IP + B[g,h,i]P)/0.5 (eq. 1)

PAHs ratio	S1	S2	Mean
An/(An+Ph)	0.08	0.05	0.07
Fl/(Fl+Py)	0.55	0.63	0.59
BaA/(BaA+Chr)	0.21	0.23	0.22
In/(BghiP+In)	0.86	0.54	0.70

Table 4. PAHs ratio index calculated in indoor dust samples

Literature data considers PAHs originating prevalently from high-temperature processes (combustion), while lower values indicate prevalently low-temperature sources (petroleum products). In our case the total index for S1 and S2 dust samples are 5.6 and 5.2, respectively, indicating a PAH profile emitted from high-temperature processes. In addition, the similarity of PAH emission and Total Index was identified in a previous study by Orecchio [42] on PAH emission from candles.

Concerning the quantification of Pt and Pb in dust samples, the data presented in Table 3 underline the presence of both lead and platinum in the samples analyzed. However, considering that the levels of lead are hundreds of times higher than those of platinum, it is possible to assume the release of particulate matter from plaster to dust, underlining the need for procedures to preserve the cultural heritage patrimony of the Palatine Chapel.

In fact, as reported in the literature [43], platinum and lead show similar concentrations when originating from vented emissions.

Conclusions

This study provided a comprehensive chemical characterization of the mural paintings and stucco artwork in the Palatine Chapel of St. Anna, located within Ventimiglia Castle in Castelbuono. By employing a combination of in situ and laboratory-based analytical techniques, critical insights were obtained into the materials, pigments, and degradation processes affecting this historic site.

X-ray diffraction (XRD) analyses suggest that the stucco artwork can be attributed to the Serpotta school, though further investigations are needed to explore potential variations in materials and techniques associated with its creation. Elemental analyses identified the presence of gold, iron, zinc, and lead in the pigments, emphasizing the historical and artistic significance of the murals. Additionally, the detection of elevated lead concentrations in dust samples underscores the urgent need for targeted conservation measures to mitigate mural painting degradation processes.

This research demonstrates the value of a multidisciplinary approach to cultural heritage conservation, integrating chemical, historical, and artistic analyses to develop a holistic understanding and effective preservation strategies. Beyond contributing to the safeguarding of the Palatine Chapel, these findings establish a methodological framework for the study and conservation of similar historical sites. This study not only contributes to the conservation of the Palatine Chapel but also sets a precedent for future research and conservation efforts in similar historical sites.

Acknowledgments

The authors are grateful to Laura Barreca and Maria Enza Puccia from Museo Civico Castelbuono.

References

- [1] T. Moutsiou, D. Ioannides, A. Charalambous, S. Schöder, S. M. Webb, M. Thoury, C. Reepmeyer, *X-ray Fluorescence Spectroscopy of Picrolite Raw Material on Cyprus*, **Heritage**, **5**(2), 2022, pp. 664-676. https://doi.org/10.3390/heritage5020037.
- [2] P. Fermo, V. Comite, Indoor air quality in heritage and museum buildings, In: Handbook of Cultural Heritage Analysis (Eds: S. D'Amico, V. Venuti), Springer International Publishing, Cham, Switzerland, 2022, pp. 1003-1031. https://doi.org/10.1007/978-3-030-60016-7 34.
- [3] S. Barreca, M. Bruno, L. Oddo, L. S. Orecchio, *Preliminary study on analysis and removal of wax from a Carrara marble statue*, **Natural Product Research**, **33**(7), 2019, pp. 947-955. https://doi.org/10.1080/14786419.2015.1113411.
- [4] D. Anelli, F. Tajani, Valorization of cultural heritage and land take reduction: An urban compensation model for the replacement of unsuitable buildings in an Italian UNESCO site, Journal of Cultural Heritage, 57, 2022, pp. 165-172. https://doi.org/10.1016/j.culher.2022.08.006.
- [5] A. Kriznar, J. Želinská, *Materials and Techniques of Selected Mural Paintings on the* "Gothic Road" Around 1400 (Slovakia), Heritage, 4(4), 2021, pp. 4105-4125. https://doi.org/10.3390/heritage4040226.
- [6] D. Jiménez-Desmond, J. S. Pozo-Antonio, A. Arizzi, *The fresco wall painting techniques in the Mediterranean area from antiquity to the present: A review*, **Journal of Cultural Heritage**, **66**, 2024, pp. 166-186. https://doi.org/10.1016/j.culher.2023.11.018.
- [7] D. Hradil, T. Grygar, J. Hradilová, P. Bezdička, Clay and iron oxide pigments in the history of painting, Applied Clay Science, 22(5), 2003, pp. 223-236. https://doi.org/10.1016/S0169-1317(03)00076-0.
- [8] B. Megna, G. Rizzo, L. Ercoli, Characterization of Serpotta's stuccos by means of simultaneous thermal analysis: Preliminary results, International Journal of Conservation Science, 6(1), 2015, pp. 1-10.
- [9] G. Montana, F. Ronca, *The "recipe" of the stucco sculptures of Giacomo Serpotta*, **Journal of Cultural Heritage**, **3**(2), 2002, pp. 133-144. https://doi.org/10.1016/S1296-2074(02)01169-X.
- [10] L. Cartechini, C. Miliani, L. Nodari, F. Rosi, P. Tomasin, *The chemistry of making color in art*, **Journal of Cultural Heritage**, **50**, 2021, pp. 188-210. https://doi.org/10.1016/j.culher.2021.05.002.
- [11] J. Riu, B. Giussani, Analytical chemistry meets art: The transformative role of chemometrics in cultural heritage preservation, Chemometrics and Intelligent Laboratory Systems, 247, 2024, Article Number: 105095. https://doi.org/10.1016/j.chemolab.2024.105095.
- [12] F. Falcone, A. Cinosi, G. Siviero, G. Rosatelli, Innovative methodological approach integrating SEM-EDS and TXRF microanalysis for characterization in materials science: A perspective from cultural heritage studies, Spectrochimica Acta Part B: Atomic Spectroscopy B, 218, 2024, Article Number: 106980. https://doi.org/10.1016/j.sab.2024.106980.
- [13] P. Fermo, C. A. Lombardi, A. D'Amato, V. Guglielmi, B. Giudici, A. Tomaino, P. Piacentini, *Disclosing colors and pigments on archaeological objects from the Aga Khan Necropolis (West Aswan, Egypt) through on-site analytical methods: Preliminary results*, **Heritage**, 7(9), 2024, pp. 4980-4996. https://doi.org/10.3390/heritage7090235.

- [14] A. Harth, *X-ray fluorescence (XRF) on painted heritage objects: A review using topic modeling*, **Heritage Science**, **12**(1), 2024, Article Number: 17. https://doi.org/10.1186/s40494-024-01135-2.
- [15] M. F. Alberghina, S. Schiavone, C. Greco, M. L. Saladino, F. Armetta, V. Renda, E. Caponetti, *How many secret details could a systematic multi-analytical study reveal about the mysterious fresco Trionfo della Morte?*, **Heritage**, **2**(3), 2019, pp. 2370-2383. https://doi.org/10.3390/heritage2030145.
- [16] D. Amorello, S. Barreca, S. Orecchio, S. Ferro, *Platinum in indoor settled dust matter* (homes and cars), Microchemical Journal, 123, 2015, pp. 76-83. https://dx.doi.org/10.1016/j.microc.2015.05.018.
- [17] D. Amorello, S. Barreca, E. Gulli, S. Orecchio, *Platinum and rhodium in wine samples by using voltammetric techniques*, **Microchemical Journal**, **130**, 2017, pp. 229-235. https://doi.org/10.1016/j.microc.2016.09.010.
- [18] F. Guerrero, K. Yáñez, V. Vidal, F. Cereceda-Balic, Effects of wood moisture on emission factors for PM2.5 particle numbers and particulate-phase PAHs from Eucalyptus globulus combustion using a controlled combustion chamber for emissions, Science of The Total Environment, 648, 2019, pp. 737-744. https://doi.org/10.1016/j.scitotenv.2018.08.057.
- [19] S. Orecchio, F. Bianchini, R. Bonsignore, P. Blandino, S. Barreca, D. Amorello, Profiles and sources of PAHs in sediments from an open-pit mining area in the Peruvian Andes, Polycyclic Aromatic Compounds, 36(4), 2016, pp. 429-451. https://doi.org/10.1080/10406638.2015.1005242.
- [20] H. Zhang, X. Zhang, Y. Wang, P. Bai, K. Hayakawa, L. Zhang, N. Tang, Characteristics and Influencing Factors of Polycyclic Aromatic Hydrocarbons Emitted from Open Burning and Stove Burning of Biomass: A Brief Review, International Journal of Environment Research and Public Health, 19(7), 2022, Article Number: 3944. https://doi.org/10.3390/ijerph19073944.
- [21] J. J. Łucejko, F. Modugno, M. P. Colombini, M. Zborowska, *Archaeological wood from the Wieliczka Salt Mine Museum, Poland—Chemical analysis of wood degradation by Py(HMDS)-GC/MS*, **Journal of Cultural Heritage**, **13**(3), 2012, pp. S50-S56. https://doi.org/10.1016/j.culher.2012.03.012.
- [22] S. Orecchio, D. Amorello, R. Indelicato, S. Barreca, S. Orecchio, A Short Review of Simple Analytical Methods for the Evaluation of PAHs and PAEs as Indoor Pollutants in House Dust Samples, Atmosphere, 13(11), 2022, 1799.
- [23] N. D. Dat, M. B. Chang, Review on Characteristics of PAHs in Atmosphere, Anthropogenic Sources and Control Technologies, Science of The Total Environment, 609, 2017, pp. 682-693. https://doi.org/10.1016/j.scitotenv.2017.07.204.
- [24] L. Yang, H. Zhang, X. Zhang, W. Xing, Y. Wang, P. Bai, N. Tang, Exposure to Atmospheric Particulate Matter-Bound Polycyclic Aromatic Hydrocarbons and Their Health Effects: A Review, International Journal of Environment Research and Public Health, 18, 2021, Article Number: 2177. https://doi.org/10.3390/ijerph18042177.
- [25] A. K. Huba, M. F. Mirabelli, R. Zenobi, *High-throughput screening of PAHs and polar trace contaminants in water matrices by direct solid-phase microextraction coupled to a dielectric barrier discharge ionization source*, **Analitica Chimica Acta**, **1030**, 2018, pp. 125-132. https://doi.org/10.1016/j.aca.2018.05.050.
- [26] J. N. Edokpayi, J. O. Odiyo, O. E. Popoola, T. A. Msagati, Determination and Distribution of Polycyclic Aromatic Hydrocarbons in Rivers, Sediments and Wastewater Effluents in Vhembe District, South Africa, International Journal of Environment Research and Public Health, 13(4), 2016, Article Number: 387. https://doi.org/10.3390/ijerph13040387.
- [27] Z. U. Zango, N. S. Sambudi, K. Jumbri, A. Ramli, N. H. H. Abu Bakar, B. Saad, A. Sulieman, An Overview and Evaluation of Highly Porous Adsorbent Materials for

- Polycyclic Aromatic Hydrocarbons and Phenols Removal from Wastewater, Water, 12(10), 2020, Article Number: 2921. https://doi.org/10.3390/w12102921.
- [28] C. Sun, J. Zhang, Q. Ma, Y. Chen, *Human Health and Ecological Risk Assessment of 16 Polycyclic Aromatic Hydrocarbons in Drinking Source Water from a Large Mixed-Use Reservoir*, **International Journal of Environment Research and Public Health**, **12**(11), 2015, pp. 13956-13969. https://doi.org/10.3390/ijerph121113956.
- [29] A. Bergamasco, L. Culotta, C. De Stefano, S. Orecchio, S. Sammartano, S. Barreca, *Composition, distribution, and sources of polycyclic aromatic hydrocarbons in sediments of the Gulf of Milazzo (Mediterranean Sea, Italy)*, **Polycyclic Aromatic Compounds**, **34**(4), 2014, pp. 397-424. https://doi.org/10.1080/10406638.2014.900642.
- [30] P. Montuori, E. De Rosa, F. Di Duca, B. De Simone, S. Scippa, I. Russo, M. Triassi, Polycyclic Aromatic Hydrocarbons (PAHs) in the Dissolved Phase, Particulate Matter, and Sediment of the Sele River, Southern Italy: A Focus on Distribution, Risk Assessment, and Sources, Toxics, 10(7), 2022, Article Number: 401. https://doi.org/10.3390/toxics10070401.
- [31] L. Rivoira, M. Castiglioni, N. Nurra, M. Battuello, R. M. Sartor, L. Favaro, M. C. Bruzzoniti, Polycyclic Aromatic Hydrocarbons and Polychlorinated Biphenyls in Seawater, Sediment and Biota of Neritic Ecosystems: Occurrence and Partition Study in Southern Ligurian Sea, Applied Sciences, 12(5), 2022, Article Number: 2564. https://doi.org/10.3390/app12052564.
- [32] P. Valentina, M. Michele, G. Tommaso, M. Letizia, M. M. Laura, M. Francesca, M. Cristina, *Sediment Contamination by Heavy Metals and PAH in the Piombino Channel (Tyrrhenian Sea)*, **Water**, **13**(11), 2021, Article Number: 1487. https://doi.org/10.3390/w13111487.
- [33] Y. Dong, Z. Yan, H. Wu, G. Zhang, H. Zhang, M. Yang, *Polycyclic Aromatic Hydrocarbons in Sediments from Typical Algae, Macrophyte Lake Bay, and Adjoining River of Taihu Lake, China: Distribution, Sources, and Risk Assessment*, Water, 13(4), 2021, Article Number: 470. https://doi.org/10.3390/w13040470.
- [34] J. E. Queb-Suarez, A. Ruiz-Marin, Y. Canedo-Lopez, C. A. Aguilar-Ucan, C. Montalvo-Romero, J. G. Flores-Trujillo, N. Perez-Morga, *Source Identification, Toxicity, and Persistence of PAHs in Sediment Core from a Natural Protected Area in Mexico*, **Energies**, **15**(19), 2022, Article Number: 7116. https://doi.org/10.3390/en15197116.
- [35] J. A. Ortega-Becerril, C. Suarez, D. Vázquez-Tarrío, J. Garrote, M. Gomez-Heras, Sediment Response after Wildfires in Mountain Streams and Their Effects on Cultural Heritage: The Case of the 2021 Navalacruz Wildfire (Avila, Spain), Fire, 7(2), 2024, Article Number: 52. https://doi.org/10.3390/fire7020052.
- [36] A. A. Argyri, A. I. Doulgeraki, E. G. Varla, V. C. Bikouli, P. I. Natskoulis, S. A. Haroutounian, N. G. Chorianopoulos, *Evaluation of Plant Origin Essential Oils as Herbal Biocides for the Protection of Caves Belonging to Natural and Cultural Heritage Sites*, **Microorganisms**, **9**(9), 2021, Article Number: 1836. https://doi.org/10.3390/microorganisms9091836.
- [37] A. Pennetta, G. E. De Benedetto, *New Evidence on the Reliable Use of Stable Isotopes of Bitumen Fractions in Archaeological Research*, **Molecules**, **28**(4), 2023, Article Number: 1962. https://doi.org/10.3390/molecules28041962.
- [38] J. J. Lucejko, D. Tamburini, F. Modugno, E. Ribechini, M. P. Colombini, *Analytical Pyrolysis and Mass Spectrometry to Characterise Lignin in Archaeological Wood*, **Applied Sciences**, **11**(1), 2020, Article Number: 240. https://doi.org/10.3390/app11010240.
- [39] L. Yang, G. Suzuki, L. Zhang, Q. Zhou, X. Zhang, W. Xing, N. Tang, *The Characteristics of Polycyclic Aromatic Hydrocarbons in Different Emission Source Areas in Shenyang*,

- *China*, International Journal of Environment Research and Public Health, 16(16), 2019, Article Number: 2817. https://doi.org/10.3390/ijerph16162817.
- [40] P. Baumard, H. Budzinski, P. Garrigues, H. Dizer, P. D. Hansen, *Polycyclic aromatic hydrocarbons in recent sediments and mussels (Mytilus edulis) from the Western Baltic Sea: Occurrence, bioavailability, and seasonal variations*, **Marine Environmental Research**, **47**(1), 1999, pp. 17-47. https://doi.org/10.1016/S0141-1136(98)00105-6.
- [41] M. B. Yunker, R. W. Macdonald, R. Vingarzan, R. H. Mitchell, D. Goyette, S. Sylvestre, *PAHs in the Fraser River basin: A critical appraisal of PAH ratios as indicators of PAH source and composition*, **Organic Geochemistry**, **33**(4), 2002, pp. 489-515. https://doi.org/10.1016/S0146-6380(02)00002-5.
- [42] S. Orecchio, *Polycyclic aromatic hydrocarbons (PAHs) in indoor emission from decorative candles*, **Atmospheric Environment**, **45**(10), 2011, pp. 1888-1895. https://doi.org/10.1016/j.atmosenv.2010.12.024.
- [43] W. Juan, R. H. Zhu, Y. Z. Shi, Distribution of platinum group elements in road dust in the Beijing metropolitan area, China, **Journal of Environmental Sciences**, **19**(1), 2007, pp. 29-34. https://doi.org/10.1016/S1001-0742(07)60005-9.

Received: November 20, 2024 Accepted: September 18, 2025